


# Design of Continuously-Adjustable Light-Scanning Handheld Probe for Photoacoustic Imaging

Yongjian Zhao , Li Liu , Ang Li, Luyao Zhu, Hengrong Lan , and Fei Gao , *Member, IEEE*

**Abstract**—To form various images at multiple locations for achieving bright- and dark-illumination fields transformation and registration-free image fusion, we proposed a continuously-adjustable light-scanning handheld probe with overall size of  $60 \times 45 \times 80 \text{ mm}^3$  for photoacoustic imaging (PAI). It has a significant advantage for image acquisition under different illumination schemes using motor driving. Specifically, a light adjustment unit was designed to produce light spots, which is more compatible with ultrasonic transducer detection region. Afterwards, multiple PA images revealing diverse features with different optical illumination regions were acquired. Consequently, the fused image was obtained with higher SNR and fidelity than respective PA image. Furthermore, both phantom and *ex-vivo* experiments were conducted to evaluate imaging performance of the developed probe. Experimental results show that SNR of the fused PA image improves by 36.06% in agar-milk phantom and 44.69% in *ex-vivo* chicken breast, respectively. Therefore, the proposed PAI handheld probe can achieve our goals well; the registration-free image fusion achieved by adaptive scanning strategy can perform better and demonstrate comprehensive features of the same imaging target.

**Index Terms**—Photoacoustic imaging, adjustable, handheld, image fusion, light scanning.

## I. INTRODUCTION

NOWADAYS, medical imaging technologies are developing very rapidly, among which photoacoustic imaging (PAI), an emerging non-invasive and non-ionizing imaging technique, attracts increasing attention in recent years [1]–[3]. In PAI, the chromogenic group in tissue is illuminated by a short-pulse laser, and then the laser-induced pressure waves are detected by ultrasound transducers to reconstruct an image, which reveals the distribution of the optical absorbers at the region of interest (ROI) [4]–[6]. This hybrid imaging approach combines the advantages of conventional optical imaging with

those of acoustic imaging, allowing for both molecular contrast and high spatial resolution in deep tissue [1], [7]–[9].

As for other medical imaging techniques: X-ray Imaging involves ionizing radiation and non-optimal sensitivity as well as specificity [10], [11]; Magnetic Resonance Imaging (MRI) enhances contrast and spatial resolution with huge time consumption and expensiveness [12], [13]; Ultrasonic Imaging (US) is non-invasive and low-cost, but the image quality requires enhancement and the false positive rate is high [14]. Compared to these state-of-the-art techniques, PAI is complementary to other imaging modalities in contrast to mechanism, penetration, spatial resolution, and temporal resolution [11]. However, limitations such as high cost, bulky size, and mode-fixed illumination of current devices of PAI system have restricted further development in clinical application [15], [18]. With the advancement of medical devices, there is an increasing trend for designing and fabricating a compact probe with both functionality and portability [20]. When it comes to PA probe designing, it is inevitable to take both the light illumination and ultrasonic waves acquisition units into consideration [11]. Laser illumination schemes of PAI system can be divided into dark- and bright-field, as well as some transition states. For PA image reconstruction, various illumination schemes directly affect the generation of PA signal and image quality. The main classification criteria involve the relative position between laser spots and ultrasonic transducer (UT) detection area [16]–[18]. Several probe designs have been reported for investigating the influence of different illumination field on imaging quality of PAI system. The previously reported handheld probes revealed that light illumination scheme is a large impact on PAI. The dark-field illumination scheme can minimize surface interference signals and reducing their contributions to the background of deeper signals. Bai *et al.* designed a handheld probe, referred to as quasibright-field, in order to achieve better image quality. By contrast, the bright-field illumination scheme may perform better under the circumstance that the phase distortion is less [19]. In this regard, Li *et al.* [20] proposed a bright-field handheld probe for non-invasive sentinel lymph node mapping. It can produce bright photoacoustic images by using a linear ultrasonic transducer. They also improved the PAI resolution by developing a fast matching delay and sum (DAS) algorithm. More recently, Liu *et al.* [21] developed a handheld volumetric PAI system with a central-holed 2D matrix aperture, achieving real-time 3D PAI for preclinical and clinical application. All these previous works in regards to probe design only take dark-field illumination or dark-field illumination into consideration. Since each type of illumination still has its own advantages under certain circumstances, it is expected that PAI can achieve adjustable illumination modes within one probe in

Manuscript received July 1, 2021; revised August 30, 2021; accepted September 19, 2021. Date of publication September 28, 2021; date of current version October 12, 2021. This work was supported in part by ShanghaiTech under start-up Grant F0203-17-004, in part by the National Natural Science Foundation of China under Grant 61805139, in part by the Natural Science Foundation of Guangdong Province, China under Grant 2018A030310565. (Yongjian Zhao and Li Liu contributed equally to this work.) (Corresponding authors: Li Liu; Fei Gao.)

Yongjian Zhao, Luyao Zhu, Hengrong Lan, and Fei Gao are with the Hybrid Imaging System Lab, Shanghai Engineering Research Center of Intelligent Vision and Imaging, School of Information Science and Technology, ShanghaiTech University, Shanghai 201210, China (e-mail: zhaoyj1@shanghaitech.edu.cn; zhuly@shanghaitech.edu.cn; lanhr@shanghaitech.edu.cn; gaofei@shanghaitech.edu.cn).

Li Liu and Ang Li are with the Department of Electronic Engineering, Chinese University of Hong Kong, Hong Kong (e-mail: liliu@cuhk.edu.hk; psw.liang@link.cuhk.edu.hk).

Digital Object Identifier 10.1109/JPHOT.2021.3115966

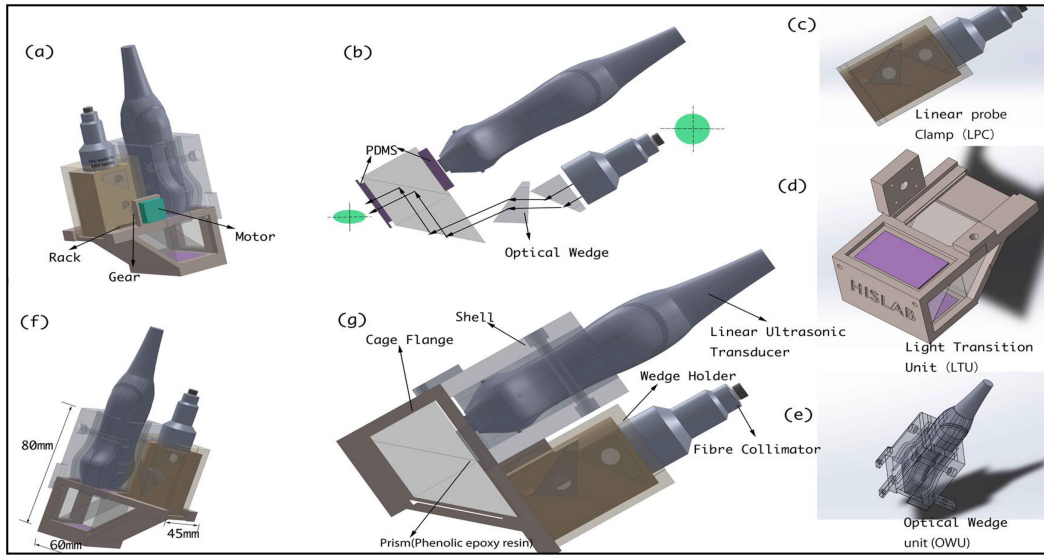


Fig. 1. CAD (Computer Aided Design) photograph of the designed handheld probe for PA imaging. (a), (f) Axonometric of probe; (b) Schematic of beam shaping; (c) Linear Probe Clamp (LPC); (d) Light Transition Unit (LTU); (e) Optical Wedge Unit (OWU); (g) Front view of probe.

order to reveal comprehensive information of the same imaging target. Specifically, the primary design principle can be summarized as: 1) **Moveable**: allowing doctors to adjust the detecting Field-of-View (FOV) freely during operation [12]. 2) **Adjustable**: switching optical exciting unit or ultrasonic receiving unit automatically via controlling unit [18], [22].

In this article, we proposed novel design of continuously-adjustable light-scanning handheld probe for PAI, which can not only acquire multiple images using moving motor based on different illumination schemes, but also can be easily suitable for single hand holding.

## II. MATERIALS AND METHODS

### A. Handheld PA Probe Design

The overall design of the PA probe is shown in Fig. 1(a)-(b). The PA probe can be divided into three parts. The first part is a medical US linear-probe clamp (LPC) as shown in Fig. 1(c). The second part is a light transition unit (LTU) as shown in Fig. 1(d), which is made up of a cage flange, a right-angle prism (Phenolic Epoxy Resin (Phenolic Epoxy Resin (Velocity:  $2670 \text{ ms}^{-1}$ , Density:  $1.03 \text{ g/cm}^{-3}$ , Acoustic impedance:  $2.75 \text{ MRayl}$ )) and an optical diffuser & acoustic delay module made of polydimethylsiloxane (PDMS), aiming to transmit both light and ultrasonic waves. The third part is an optic wedge unit (OWU) for light beam shaping as shown in Fig. 1(e) (Material: SR11, refractive index: 1.843 at the wavelength of 532 nm, wedge angle:  $29^\circ 26'$ ) along with the mounting base, aiming at compressing the incident collimated light in one dimension to achieve the elliptical beam with the horizontal-to-vertical proportion of 3.41:1. Meanwhile, there are specified orbits on the wedge holder for connection with the cage flange. We may obtain beam shaping units with different compressing ratios by changing OWU. The dimension of the PA probe is  $60 \times 45 \times 80 \text{ mm}^3$  (Fig. 1(f)), and it can be held by an adult's single hand as shown in Fig. 2(a)-(b). In order to control the PA probe, we

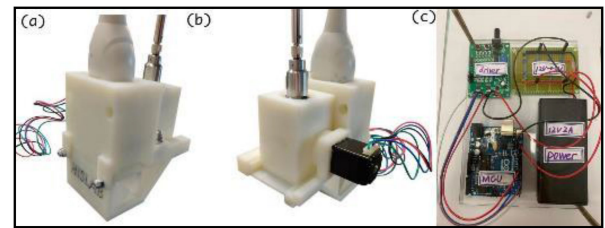


Fig. 2. Photograph of the assembled handheld PA probe. (a-b) External structure of probe; (c) Control board.

devised a control board based on Arduino platform consisting of a power module, a driver module and a voltage conversion module as shown in Fig. 2(c).

An optically transparent Poly (vinylidene chloride) membrane covers the diffusing pad to protect the gel from desiccation and mechanical damage, facilitating relatively rough handheld operation. Compatible with handheld requirement, the free space light from the high-power pulsed laser (pulse duration: 7ns, repetition rate: 8Hz, wavelength: 532 nm, LPS-532-L, CNI) is coupled into a multi-mode fiber (FIB-1000-Duv-OSMA, Ideoptics). After travelling through the collimator (F810SMA-543, Thorlabs, USA, NA: 0.39 in air), the divergent light turns into a collimated Gaussian-beam with the diameter of 20mm and the divergence angle of 0.5mm/rad. Afterwards, the beam travels through the shaping unit, with the major axis remaining to be 20mm and the minor axis compressed to be 5.45mm. After being refracted twice, the beam reaches the sample surface and provides optical excitation. It is worth noting that the OWU moving along the orbit is driven by a stepper motor fixed on the cage flange to provide rotational power input, where the OWU is connected to a rack with a common mode with the gear. Moving the OWU along the orbit, we can adjust the positions of beam excitation continuously, generating different illumination patterns of optical excitation for multiple PA image reconstruction.

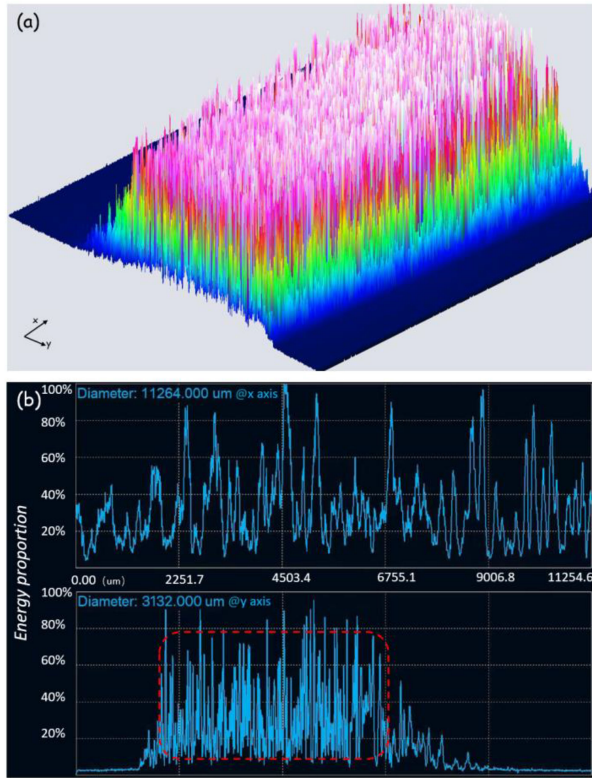


Fig. 3. Characterization of light spots (a) energy distribution. (b) spot size.

We also used beam analyzer (SP503U, Spiricon, USA) to reveal the characterization of light spots. As shown in Fig. 3, It can be easily seen that the size ratio of  $y$  by  $x$  is  $\sim 359$ , which is close to the ideal ratio 3.41.

### B. Numerical Simulation

To evaluate light illumination performance of the proposed probe, 3D fluence map within the region of interest (ROI) was estimated through the Monte Carlo simulation using Monte Carlo extreme (MCX) package [23]. We set the light source as an oval planar pattern, and there are two layers of the simulating media: the upper one being PDMS ( $60 \times 60 \times 5 \text{ mm}^3$ ) and the lower one being a tissue-mimicking medium ( $60 \times 60 \times 60 \text{ mm}^3$ ) for light propagation. The parameters of the PDMS layer are: refractive index  $n$ : 1.41@532 nm, absorption coefficient:  $0.001 \text{ mm}^{-1}$ , scattering coefficient:  $0.1 \text{ mm}^{-1}$ . Parameters of the tissue-mimicking medium are refractive index  $n$ : 1.35, absorption coefficient:  $0.003 \text{ mm}^{-1}$ , and scattering coefficient:  $0.15 \text{ mm}^{-1}$ . Moreover, we set two optical absorbers in the medium with the intervals of 20 mm in  $z$ -direction (cylinder, radius being 3 mm,  $z$ -coordinates being 55 mm, 35 mm). The parameters of the two absorbers are: refractive index  $n$ : 1.54, absorption coefficient:  $0.01 \text{ mm}^{-1}$ , scattering coefficient:  $10 \text{ mm}^{-1}$ . By gradually scanning the position of the light source to simulate the working process of the probe, we obtained a set of optical fluence distribution images as shown in Fig. 4. Moreover, Fig. 5 indicates homogenization energy of MC simulation. It is observed that on the beginning location under 3 mm depth collects more photons due to illumination light on the top of the absorber (Fig 4(a)). On the deeper location, the absorber

receives more photons compared with beginning location when light illuminates sample on the side direction (Fig 4(b) & (c)).

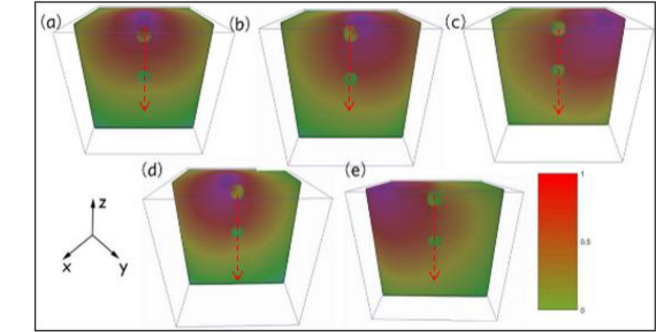


Fig. 4. Simulation results of laser fluence at different illumination locations in tissue mimicking medium. (a) Light from directly above; (b)~(c) Light from the right; (d)~(e) Light from the left.

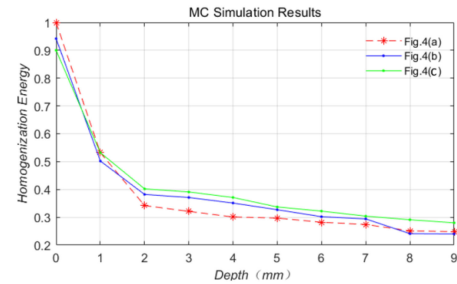


Fig. 5 Homogenization Energy of MC Simulation.

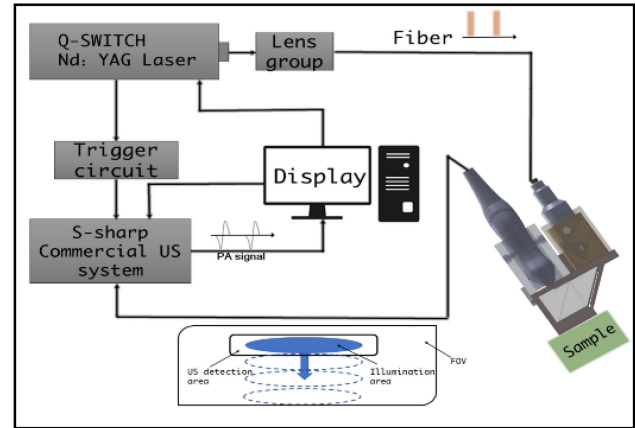


Fig. 6. Schematic of the PA imaging system based on the proposed hand-held probe. (b)~(c) Light from the right; (d)~(e) Light from the left.

receives more photons compared with beginning location when light illuminates sample on the side direction (Fig 4(b) & (c)).

### C. Experimental Setup

The experimental setup is shown in Fig. 6. The Q-switch pulsed laser is used for optical excitation with fiber coupling. After laser illumination on the sample, the induced PA wave passed through the PDMS and the prism layers, then reached the medical US linear array probe, followed by data acquisition (DAQ) using a US imaging system (S-Sharp) for further processing and image reconstruction. A computer is used to synchronize the laser irradiation and acoustic data acquisition. The PA imaging speed is about 8 frames/sec limited by the repetition rate of laser source. The stepper motor is set to

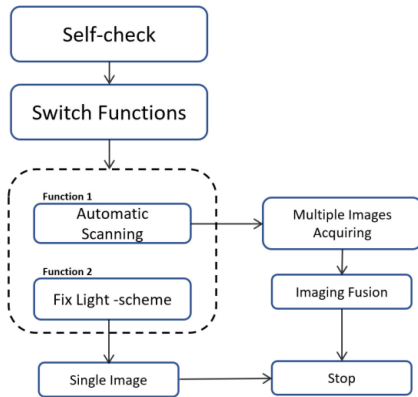


Fig. 7. Workflow of light-scanning probe.

16 subdivisions, which means that each pulse rotates 0.1125 degrees, and the motor speed is set to 60 r/min. There are in total 6 detection positions, and the motor movement time between each position is 0.17s, and the stop interval of each position is 3s for image acquisition. We achieved 48 images for in total 6 positions spending 3.127s on image acquisition, reconstruction and fusion. Therefore, it took a total of 18.977s to conduct the scanning process including motor movement and image processing. We can regard it as a real-time imaging probe with an imaging speed of 8 frames per second (limited by the repetition frequency of the laser). During implementation of the real-time imaging, we will further consider the adjustable bright- and dark-field for this probe. Researchers can choose bright-field or dark-field irradiation to satisfy experimental requirements. For those experiments only for static imaging, the designed PAI probe can realize the function of multi-image fusion. This can provide more information on the same image in the same experiment. The Fig. 6 also demonstrates the relative position between the US detection area and the illumination area. The US area stays still while the illumination area moves with the OWU.

Fig. 7 shows the workflow of the proposed system. the user can switch two different schemes after the probe is self-checked. One is automatic scanning while the other is associated with fixed light scheme. The former indicates that the system can scan sample and acquire multiple images for fusion. By contrast, the fixed light scheme provides a function that can realize bright- or dark- field through user-defined critical parameters, and various images with different illumination will be obtained subsequently.

#### D. Phantom Study

We designed an agar-milk phantom for testing the designed probe as shown in Fig. 8(a). Two cylinders were 3D printed with the diameters of 1 mm and lengths of 15 mm as optical absorbers (UV Curable Resin), which were immersed into 5% black ink (absorption coefficient  $\sim 108\text{cm}^{-1}$ ) for dyeing uniformly. Mixing 5g pure milk with 60g distilled water to produce the scattering medium, we boiled the solution with an induction cooker and added 2g agar power at the same time, followed by stirring constantly for the acquisition of the agar-milk solution. The two absorbers were vertically inserted into the solution, parallel to

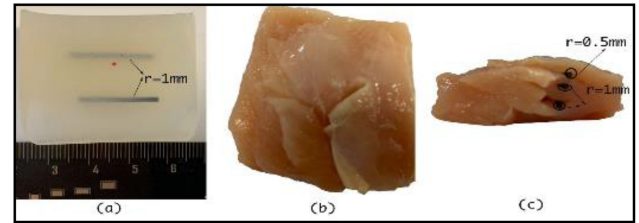


Fig. 8. Photographs of phantom. (a) agar-milk phantom (b)~(c) chicken breast phantom. (b)~(c) Light from the right; (d)~(e) Light from the left.

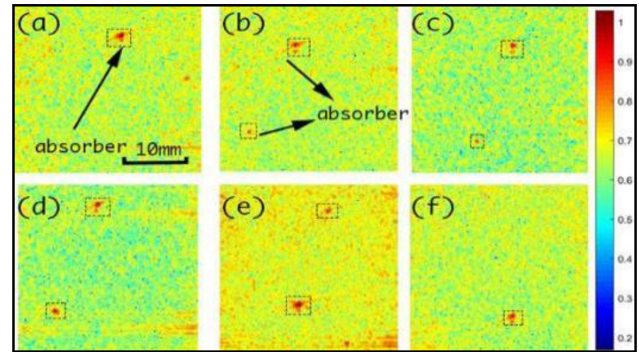


Fig. 9. The agar-milk phantom imaging results with different illumination locations in parallel detection mode: (a) light and ultrasound area are overlapped (Bright-field), (b)~(d) The distance between light and ultrasound area : 1 cm, 2 cm, and 3 cm away from the center zone.

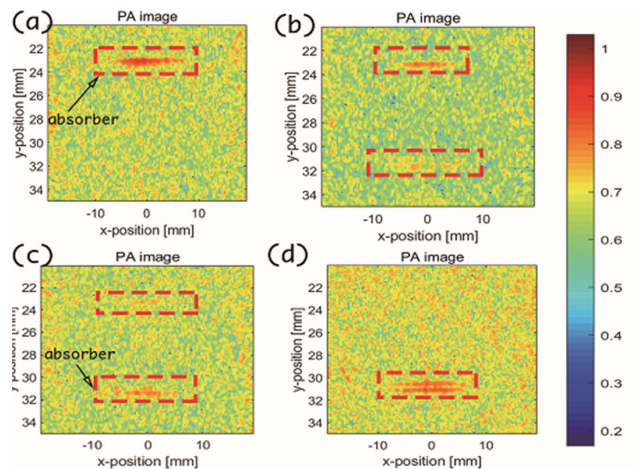


Fig. 10. The agar-milk phantom imaging results with different illumination locations in vertical detection mode: (a) light and ultrasound area are overlapped (Bright-field); (b)~(d) distance between light and ultrasound area: 1 cm, 2 cm, and 3 cm away from the central zone.

each other with the interval of 10 mm. The phantom was poured into the specific mold to solidify for the experiment. In this paper, we evaluated two detection methods, where one is that the probe detection area and the absorber are detected in parallel, and the other is that the probe and the absorber are placed vertically in space to observe the detection results. The results are shown in Fig. 9 & 10.

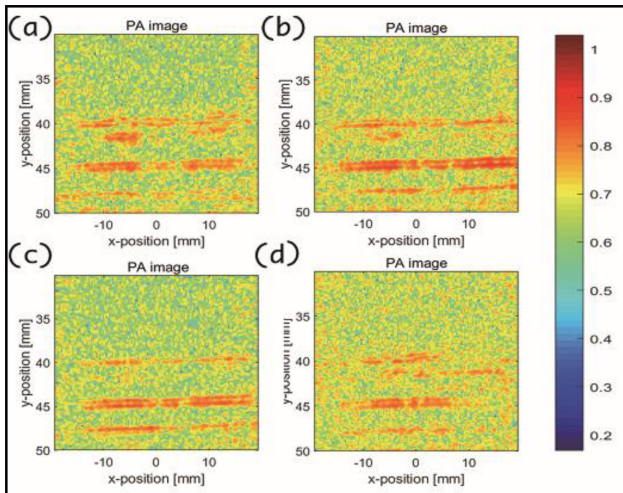


Fig. 11. Experimental results on chicken-breast phantom corresponding to different illumination locations: (a) light and ultrasound area are overlapped (Bright-field); (b)–(d) distance between light and ultrasound area: 1 cm, 2 cm, and 3 cm away from the central zone.

### E. Ex Vivo Study

In order to further evaluate the performance of the PAI probe, we used chicken breast for *ex vivo* phantom study. We picked up the fresh chicken breast with 50g as the sample. The muscles at different depths were divided along the fiber texture using surgical forceps. Two different kinds of black rubber sticks were selected as the optical absorbers with diameters 0.5 mm and 1.0 mm, respectively. The 0.5 mm stick was set on the uppermost layer, while the two 1.0 mm sticks were set on the two lower layers, each being 5.0 mm apart from the upper one. Afterwards, the muscles were cautiously rehabilitated, and the fabricated sample was shown in Fig. 8(b)~(c).

## III. RESULTS

We conducted experiments using both the agar phantom and the chicken breast phantom. The probe was held by hand, and the samples were attached to the detection region coated with the US coupling gel. Afterwards, we started the motor for controlled scanning. The acquired data was loaded into MATLAB for image reconstruction and fusion, without needing for image registration since the relative position of the probe and the samples was unchanged. The imaging results of the agar phantom were shown in Fig. 9 & 10, while those of the chicken breast phantom and the fused image were shown in Fig. 11 and Fig. 12, respectively. The last two images of the experiment were abandoned. The remained four images were used to characterize the results of the PA imaging.

### A. Phantom Results

As shown in Fig. 9 and Fig. 10, when the light was directly over the samples (Fig. 9 & 10(a)), the upper absorber was clearly demonstrated, while the lower one showed very weak PA signals since it received much fewer photons due to the shielding of upper absorber. As the light spot moved away from the confocal zone, the PA signals of the upper absorber reduced gradually, while that of the lower one is enhanced (Fig. 9 & 10(b)–(c)). The reason is that as the relative displacement between the beam

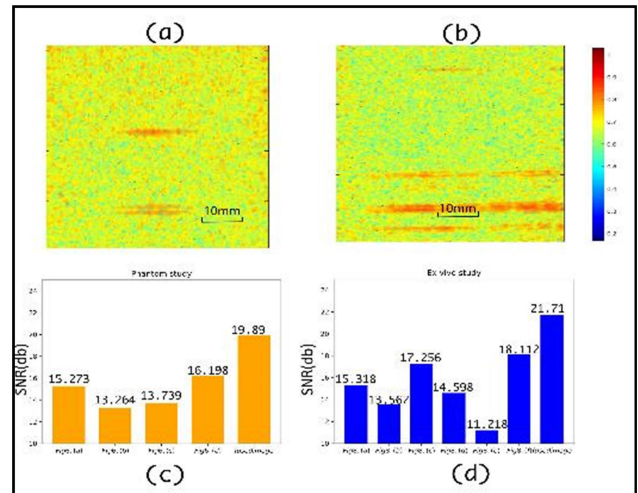


Fig. 12. Fused images for both experiments: (a) agar-milk phantom, (b) chicken breast phantom, and (c) quantitative evaluation of PA images before and after image fusion.

and absorber increases, the upper absorber receives less and less photons. On the other hand, the lower one might receive more light. Equivalently, the illumination pattern is gradually switching from bright-field to dark-field illumination. When the illumination arrives the boundary of sample, as shown in Fig. 9 & 10(d), the lower absorber generates stronger PA signal due to more photon irradiation.

### B. Ex Vivo Experiment Results

Fig. 11 shows the chicken breast imaging results, where we obtained 4 images showing the positions and outlines of the three absorbers. (y axis reflects the distance between the absorber and surface of the UT. This distance includes a 20 mm epoxy layer, which is a common acoustic lens material, and there will be lower sound wave attenuation in this material.) The lowest absorber shows weakest signals due to its large depth, and the middle absorber demonstrated the strongest signals in Fig. 11(a) and (b). As the light spot moved, the middle absorber's signal decreased while the lowest one is slight enhanced. We may conclude that we can acquire PA images with different emphases through the light scanning mechanism, which provides more details.

### C. Image Fusion Method and Results

According to the different ways of applying image information processing, image fusion can be divided into three levels, namely pixel level, feature level and decision level. Among them, the pixel-level fusion is located at the lowest layer, which can be regarded as only extracting the information and using it directly. It is also because of its maximum retention of information that it is superior to the other two levels in accuracy and robustness. In contrast, pixel-level fusion obtains more detailed information and is the most commonly used fusion method. At the same time, because there is no sensor displacement in our image acquisition process, there is no registration problem, so it can greatly reduce the time-consuming problems caused by registration. In this paper, we use the average method for image fusion. And calculate the SNR of the image.

The formula of SNR can be stated as:

$$SNR (db) = 10 \log_{10} \times \left[ \frac{\sum_{x=1}^{N_x} \sum_{y=1}^{N_y} (f(x, y))^2}{\sum_{x=1}^{N_x} \sum_{y=1}^{N_y} (f(x, y) - \bar{f}(x, y))^2} \right] \quad (1)$$

After image fusion, Fig. 12(a) shows agar-milk imaging results with the SNR growth up to 50.94%. Similarly, the image quality of chicken breast phantom is also clearly improvement, and the SNR enhancement is up to 30.93% compared with the single PA image. More importantly, all the absorber can be clearly identified in the fused image with high contrast. Moreover, since there is no relative displacement for the US transducer and the sample, no image registration is needed, ensuring easy-to-use operation and low computation cost.

#### IV. DISCUSSION

Different lighting schemes can demonstrate different information on an unified target object. Therefore, in this paper, designing a light scanning probe for PA imaging, we carried out a series of experiments to verify the functions of the proposed probe. Generally, if researchers want to show the contours of deeper objects, one conventional way in their schemes is to increase the energy of laser, aiming to deliver more photons to deeper tissues. Unfortunately, this way can make laser energy in per unit area arrive in or beyond the safety standard, increasing the risks of harm of tissue surface. Meanwhile, due to the scattering effect of tissue, it will produce a phenomenon where the superficial tissue obtains too much energy, causing overexposed effect, while deeper tissue still has no enough photons for ultrasonic excitation.

To address this problem and similarly meet the requirements of clinical usefulness, the best way is to adjust the illumination schemes according to different samples. In this paper, we designed a continuously-adjustable light-scanning probe which can produce different light schemes. Because scattering coefficient differs from the types of samples. For the superficial imaging target, the ideal light scheme is bright field imaging, since it can provide high contrast with lower laser energy. However, it is obvious that for the imaging requirements of large imaging depth, images with different focus information will be generated under the same energy density illumination, which also means that for each image, the rest of the information will be lost as well. The missing information in some pictures will also be found in the rest of the images. In this case, when we performed an image fusion operation, an image with global information will be generated in the same image for subsequent analysis.

#### V. CONCLUSION

In this paper, the light scanning adjustable handheld PAI probe is proposed, which can realize PA imaging with different illumination positions via adjusting the optical unit. In order to achieve the matched beam shape with the US detection area, a couple of optical wedges were used to realize the compressing ratio of 3.41:1. The MCX simulation results revealed that the absorbers of different depth position would receive different amounts of photons. And this proposed PAI probe can adjust the illumination area without changing relative position between the US transducer and the sample. Both the agar-milk and

the chicken breast phantom imaging results demonstrated the position and the contour of the absorbers. Moreover, based on image fusion, the SNR of the resulting image is increased by 36.06% and 44.69%, respectively compared to the average SNR of the pre-processed image. Experimental results demonstrated the high feasibility and potential for clinical translation.

#### REFERENCES

- [1] Z. Xie *et al.*, "In vivo assessment of inflammation in carotid atherosclerosis by noninvasive photoacoustic imaging," *Theranostics*, vol. 10, no. 10, pp. 4694–4704, 2020.
- [2] J. Yao *et al.*, "High-speed label-free functional photoacoustic microscopy of mouse brain in action," *Nature Methods*, vol. 12, no. 5, pp. 407–410, May 2015.
- [3] L. V. Wang and S. Hu, "Photoacoustic tomography: In vivo imaging from organelles to organs," *Science*, vol. 335, no. 6075, 2012, Art. no. 1458.
- [4] T. Zhao, A. E. Desjardins, S. Ourselin, T. Vercauteren, and W. Xia, "Minimally invasive photoacoustic imaging: Current status and future perspectives," *Photoacoustics*, vol. 16, 2019, Art. no. 100146.
- [5] A. Swamy *et al.*, "Validation of diffuse reflectance spectroscopy with magnetic resonance imaging for accurate vertebral bone fat fraction quantification," *Biomed Opt. Exp.*, vol. 10, no. 8, pp. 4316–4328, Aug. 1, 2019.
- [6] L. V. Wang and J. Yao, "A practical guide to photoacoustic tomography in the life sciences," *Nat. Methods*, vol. 13, no. 8, pp. 627–638, Jul. 28, 2016.
- [7] H. Zhong, D. Jiang, T. Duan, H. Lan, J. Zhang, and F. Gao, "Fingertip laser diode system enables both time-domain and frequency-domain photoacoustic imaging," in *Proc. IEEE Int. Symp. Circuits Syst.*, 2019, pp. 1–4.
- [8] C. Tian, M. Pei, K. Shen, S. Liu, Z. Hu, and T. Feng, "Impact of system factors on the performance of photoacoustic tomography scanners," *Phys. Rev. Appl.*, vol. 13, no. 1, 2020, Art. no. 014001.
- [9] M. W. Schellenberg and H. K. Hunt, "Hand-held optoacoustic imaging: A review," *Photoacoustics*, vol. 11, pp. 14–27, Sep. 2018.
- [10] S. Manohar and M. Dantuma, "Current and future trends in photoacoustic breast imaging," *Photoacoustics*, vol. 16, Dec. 2019, Art. no. 100134.
- [11] N. Nyayapathi and J. Xia, "Photoacoustic imaging of breast cancer: A mini review of system design and image features," *J. Biomed. Opt.*, vol. 24, no. 12, pp. 1–13, Nov. 2019.
- [12] I. Steinberg, D. M. Huland, O. Vermesh, H. E. Frostig, W. S. Tummers, and S. S. Gambhir, "Photoacoustic clinical imaging," *Photoacoustics*, vol. 14, pp. 77–98, Jun. 2019.
- [13] C. K. Kuhl *et al.*, "Mammography, breast ultrasound, and magnetic resonance imaging for surveillance of women at high familial risk for breast cancer," *J. Clin. Oncol.*, vol. 23, no. 33, pp. 8469–8476, Nov. 2005.
- [14] J. Xia and L. V. Wang, "Small-animal whole-body photoacoustic tomography: A review," *IEEE Trans. Biomed. Eng.*, vol. 61, no. 5, pp. 1380–1389, May 2014.
- [15] P. Beard, "Biomedical photoacoustic imaging," *Interface Focus*, vol. 1, no. 4, pp. 602–631, Aug. 6, 2011.
- [16] J. Zhang, B. Chen, M. Zhou, H. Lan, and F. Gao, "Photoacoustic image classification and segmentation of breast cancer: A feasibility study," *IEEE Access*, vol. 7, pp. 5457–5466, 2019.
- [17] Y. Zhou, W. Xing, K. I. Maslov, L. A. Cornelius, and L. V. Wang, "Handheld photoacoustic microscopy to detect melanoma depth in vivo," *Opt. Lett.*, vol. 39, no. 16, pp. 4731–4734, 2014.
- [18] Y. Zhao, D. Jiang, H. Lan, and F. Gao, "Image infusion of photoacoustic imaging based on novel adjustable hand-held probe," in *Proc. IEEE Int. Ultrasonics Symp.*, 2019, pp. 2366–2368.
- [19] Y. Bai, B. Cong, X. Gong, L. Song, and C. Liu, "Compact and low-cost handheld quasibright-field linear-array probe design in photoacoustic computed tomography," *J. Biomed. Opt.*, vol. 23, no. 12, 2018, Art. no. 121606.
- [20] M. Li *et al.*, "Linear array-based real-time photoacoustic imaging system with a compact coaxial excitation handheld probe for noninvasive sentinel lymph node mapping," *Biomed. Opt. Exp.*, vol. 9, no. 4, 2018, Art. no. 1408.
- [21] S. Liu, W. Song, X. Liao, T. H. Kim, and Y. Zheng, "Development of a handheld volumetric photoacoustic imaging system with a central-holed 2D matrix aperture," *IEEE Trans. Biomed. Eng.*, vol. 67, no. 9, pp. 2482–2489, Sep. 2020.
- [22] G. S. Sangha and C. J. Goergen, "Photoacoustic tomography: Applications for atherosclerosis imaging," *J. Opt.*, vol. 18, no. 8, 2016, Art. no. 084005.
- [23] Q. Fang, "Mesh-based Monte Carlo method using fast ray-tracing in plücker coordinates," *Biomed. Opt. Exp.*, vol. 1, pp. 165–175, 2010.